atoms

MDPI

Article

Integral Cross Sections and Transport Properties for Electron–Radon Scattering over a Wide Energy Range (0–1000 eV) and a Reduced Electric Field Range (0.01–1000 Td)

Gregory J. Boyle [1,*], Dale L. Muccignat [1], Joshua R. Machacek [2,*] and Robert P. McEachran [2]

[1] College of Science and Engineering, James Cook University, Townsville, QLD 4810, Australia; dale.muccignat@jcu.edu.au
[2] Research School of Physics, Australian National University, Canberra, ACT 0200, Australia; robert.mceachran@anu.edu.au
* Correspondence: gregory.boyle@my.jcu.edu.au (G.J.B.); joshua.machacek@anu.edu.au (J.R.M.)

Abstract

We report calculations for electron–radon scattering using a complex relativistic optical potential method. The energy range of this study is 0–1000 eV, with results for the elastic (total, momentum-transfer and viscosity-transfer) cross section, summed discrete electronic-state integral excitation cross sections and electron-impact ionization cross sections presented. Here, we obtain our cross sections from a single theoretical relativistic calculation. Since radon is a heavy element, a relativistic treatment is very desirable. The electron transport coefficients are subsequently calculated for reduced electric fields ranging from 0.01 to 1000 Td, using a multi-term solution of Boltzmann's equation.

Keywords: radon; electron scattering; electron transport

check for updates

Academic Editor: David D. Reid

Received: 14 July 2025
Revised: 12 September 2025
Accepted: 18 September 2025
Published: 23 September 2025

Citation: Boyle, G.J.; Muccignat, D.L.; Machacek, J.R.; McEachran, R.P. Integral Cross Sections and Transport Properties for Electron–Radon Scattering over a Wide Energy Range (0–1000 eV) and a Reduced Electric Field Range (0.01–1000 Td). *Atoms* **2025**, *13*, 82. https://doi.org/10.3390/atoms13100082

1. Introduction

Noble gases, with their closed outer shells, provide a testbed for benchmarking theoretical techniques over a large range of electron numbers. For the lightest noble gas, He, accurate theory and experiments are in agreement for electron [1] elastic scattering. Radon is the heaviest naturally occurring closed-shell atom. It is produced during the decay of Uranium and is unstable to alpha decay, with a lifetime of 3.8 days ($_{222}$Rn). This short lifetime to alpha decay, and the toxicity of the decay products, imposes severe difficulties onto experimental investigations. Thus, to date, no electron scattering experiments have been conducted. However, theoretical studies of scattering processes exist for electrons [2–5].

We begin this paper by describing the theory for the cross section calculations using the complex relativistic optical potential (ROP) method and the details of the transport theory and simulation in Section 2. The cross section calculations are presented and compared to the optical potential method (OPM) calculations of Khandker et al. (2021) [2] in Section 3.1. The corresponding transport properties are presented in Section 3.2 and compared with experimental measurements where available. Finally, the results are summarized in Section 4.

2. Theoretical Scattering and Transport Simulation Details

2.1. Cross Sections

The theoretical method used here to describe the elastic and inelastic scattering of electrons from radon atoms is based upon the relativistic optical potential (ROP) method of Chen et al. (2008) [6]. This optical potential method is based upon an approximate solution of the relativistic close-coupling equations and has recently been used to describe electron scattering from helium [7]. Consequently, only a brief discussion of the overall method will be given here, and the reader is referred to ref. [6] for details.

The scattering of the incident electron, with the wavenumber k, by radon atoms is described by an integral equation formulation of the partial wave Dirac–Fock scattering equations. In the ROP method, these equations can be written in matrix form as

$$\begin{pmatrix} F_k(r) \\ G_k(r) \end{pmatrix} = \begin{pmatrix} v_1(kr) \\ v_2(kr) \end{pmatrix} + \frac{1}{k}\int_0^r dx\, G(r,x)\left[\left(U(x) - iU_{\mathrm{opt}}(x)\right)\begin{pmatrix} F_k(x) \\ G_k(x) \end{pmatrix} - \begin{pmatrix} \overline{W}_Q(k;x) \\ \overline{W}_P(k;x) \end{pmatrix}\right], \quad (1)$$

where the local potential $U(r)$ is given by the sum of static and local polarization potential plus an additional dynamic distortion potential, i.e.,

$$U(r) = U_{\mathrm{st}}(r) + U_{\mathrm{pol}}(r) + \tfrac{1}{2}\, U_{\mathrm{d}}(r). \quad (2)$$

Furthermore, the terms $\overline{W}_P$ and $\overline{W}_Q$ are the large and small components of the non-local exchange terms. Finally, $U_{\mathrm{opt}}(r)$ is the optical potential, which accounts for the inelastic processes, as discussed below. The Dirac–Fock scattering equations were solved by numerically integrating out from the origin using a four-stage equidistant mesh of an increasing size.

The static potential was determined in the usual manner from the ground state Dirac–Fock orbitals of radon. The polarization potential $U_{\mathrm{pol}}(r)$ in Equation (2) comprised the sum of the first eight multipole polarization potentials, which were determined using the polarized-orbital method of McEachran et al. [8,9]. The dynamic distortion potential was determined using the method outlined in McEachran and Stauffer [10,11].

Here, we have also used the procedure outlined by Bartschat et al. [12,13], whereby the real part of the complex optical potential $U_{\mathrm{opt}}(r)$ was replaced by the local polarization potentials $U_{\mathrm{pol}}(r)$ based upon the polarized-orbital method. Thus, in Equation (1), the non-local potential $U_{\mathrm{opt}}(r)$ denotes just the imaginary part of the optical potential, which, in turn, describes the absorption of the incident flux into the inelastic channels and thereby describes both excitation and ionization processes.

Finally, in Equation (1), $F_k(r)$ and $G_k(r)$ are the large and small components of the complex scattering wavefunctions, while the functions $v_1(kr)$ and $v_2(kr)$ are the corresponding free particle wavefunctions and are given in terms of Riccati–Bessel functions. Here, $G(r,x)$ is the free particle Green's function, which can be expressed in matrix form in terms of the Riccati–Bessel and Riccati–Neumann functions (see Equation (23) of ref. [6] for details). The subscript k on the scattering wavefunctions and in the argument of the exchange terms is the relativistic angular momentum quantum number of the incident particle. It is related to the corresponding orbital angular momentum quantum number l according to $k = -l - 1$ when $j = l + \frac{1}{2}$ (spin-up) and $k = l$ when $j = l - \frac{1}{2}$ (spin-down), where j is the total angular momentum quantum number of the incident particle.

The large component of the complex scattering wavefunction is given asymptotically by

$$F_k(x \to \infty) = \sin\left(kx - \frac{l\pi}{2}\right) + T_l^{\pm}(k)\exp\left(kx - \frac{l\pi}{2}\right), \quad (3)$$

where $T_l^{\pm}(k)$ are the complex T-matrix elements. These T-matrix elements can be expressed in terms of the complex phase shifts $\eta_l^{\pm}(k)$ according to

$$T_l^{\pm}(k) = \frac{1}{2i}\left[\exp\left(2i\eta_l^{\pm}(k)\right) - 1\right], \quad (4)$$

where the real and imaginary parts of the phase shifts are given by

$$\eta_l^{\pm}(k) = \delta_l^{\pm}(k) + i\,\gamma_l^{\pm}(k). \tag{5}$$

The elastic and inelastic cross sections can be found in terms of these phase shifts. The integrated elastic cross section is given by

$$\begin{aligned}\sigma^{\mathrm{el}}(k^2) = \frac{2\pi}{k^2}\sum_{l=0}^{\infty}\Big\{&(l+1)\exp(-2\gamma_l^+)\big[\cosh 2\gamma_l^+ - \cos 2\delta_l^+\big] \\ &+ l\exp(-2\gamma_l^-)\big[\cosh 2\gamma_l^- - \cos 2\delta_l^-\big]\Big\},\end{aligned} \tag{6}$$

while the total inelastic or absorption cross section is given by

$$\sigma^{\mathrm{inel}}(k^2) = \frac{\pi}{k^2}\sum_{l=0}^{\infty}\Big\{(l+1)\,\big[1-\exp(-4\gamma_l^+)\big] + l\big[1-\exp(-4\gamma_l^-)\big]\Big\}. \tag{7}$$

Here, the superscript $+$ refers to 'spin-up', while the superscript $-$ refers to 'spin-down'.

In this work, we also include anisotropic elastic scattering effects through the momentum-transfer and viscosity-transfer cross sections, which, in the elastic region (i.e., real phase shifts), are given by

$$\begin{aligned}\sigma^{\mathrm{mom}}(k^2) = \frac{4\pi}{k^2}\sum_{l=0}^{\infty}\bigg\{&\frac{(l+1)(l+2)}{(2l+3)}\sin^2(\delta_l^+ - \delta_{l+1}^+) \\ &+ \frac{l(l+1)}{(2l+1)}\sin^2(\delta_l^- - \delta_{l+1}^-) \\ &+ \frac{(l+1)}{(2l+1)(2l+3)}\sin^2(\delta_l^+ - \delta_{l+1}^-)\bigg\},\end{aligned} \tag{8}$$

and

$$\begin{aligned}\sigma^{\mathrm{vis}}(k^2) = \frac{4\pi}{k^2}\sum_{l=0}^{\infty}\bigg\{&\frac{2l(l+1)}{(2l-1)(2l+1)(2l+3)}\sin^2(\delta_l^+ - \delta_l^-) \\ &+ \frac{(l+1)(l+2)(l+3)}{(2l+3)(2l+5)}\sin^2(\delta_l^+ - \delta_{l+2}^+) \\ &+ \frac{l(l+1)(l+2)}{(2l+1)(2l+3)}\sin^2(\delta_l^- - \delta_{l+2}^-) \\ &+ \frac{2(l+1)(l+2)}{(2l+1)(2l+3)(2l+5)}\sin^2(\delta_l^+ - \delta_{l+2}^-)\bigg\},\end{aligned} \tag{9}$$

respectively.

2.2. Excitation and Ionization

For radon, the following eight bound excited states were included in $U_{\mathrm{opt}}(r)$, namely 7s$[3/2]_1$, 7s$[1/2]_1$, 7p$[1/2]_0$, 7p$[5/2]_2$, 7p$[3/2]_2$, 6$\overline{\mathrm{d}}[1/2]_1$, 6d$[3/2]_1$ and 6d$[7/2]_3$.

Also included in $U_{\mathrm{opt}}(r)$ were all continuum states with orbital angular momentum given by $l_{\mathrm{c}} = 0, 1, 2, 3$ and 4 in order to simulate the ionization processes for the 7$\overline{\mathrm{p}}$, 7p and 7s electrons. The integration over the continuum states in the absorption potential was approximated by using Gauss–Legendre integration with 16 points.

In a relativistic close-coupling expansion, it is necessary to couple the total angular momentum of the electron in the excited state (bound or continuum) to the total angular momentum of the incident particle in order to obtain the total angular momentum J of the incident particle–atom system. This total angular momentum J is then conserved during the collision process. Under these circumstances, this gave rise to a maximum of 30 excitation channels for radon. Similarly, there were 198 ionization channels in $U_{\text{opt}}(r)$.

2.3. Comparison of the ROP and OPM Methods

Both the ROP and OPM methods are based upon a relativistic formalism that involves a Dirac scattering equation; however, the overall methods are extremely different. In the ROP method, the total scattering wavefunction is antisymmetrized in order to derive the non-local exchange terms. On the other hand, in the OPM method, these terms are included via a local exchange potential. Thus, the scattering Equation (1) above includes both potential and exchange terms, whereas Equations (26) and (27) from Khandker et al. [2] only involve potential terms.

The ROP method contains a polarization potential which comprises the first eight multipole polarization potentials plus a dynamic polarization potential. These states where chosen to correspond with the most important, or strongest, dipole and quadrupole transitions. The OPM method only has a dipole polarization potential. Furthermore, the ROP polarization potentials are determined using the atomic wavefunctions and a first-order correction of these wavefunctions. In contrast, the OPM dipole polarization potential is based upon the original Buckingham polarization potential, which contains one adjustable parameter.

In the ROP method, the absorption potential is determined from the discrete and continuum Dirac–Fock wavefunctions. Alternatively, the OPM method describes inelastic processes using a semi-relativistic potential due to Salvat [14].

Radon is a very heavy and hence relativistic atom. For example, the two 7s levels, $7\text{s}[3/2]_{J=2,1}$, lie at 6.772 and 6.942 eV above the ground state, whereas the two 7s levels, $7\text{s}[1/2]_{J=0,1}$, lie just above the ionization threshold at 10.748 eV [15]. Consequently, since the ROP method uses the consistent fully relativistic atomic wavefunctions of radon to derive its representation of the polarization, exchange and absorption interactions, its result should, in principle, be more reliable.

2.4. Transport Simulations

The transport simulations presented in this work are based on a multi-term solution of Boltzmann's equation, following methods described extensively elsewhere [16–20]. Only a brief summary is provided here, and we direct the reader to the references above for a more detailed account.

The electron transport in radon gas under a uniform electric field $\mathbf{E}$ is described by Boltzmann's equation for the phase-space distribution function $f(\mathbf{r}, \mathbf{v}, t)$:

$$\frac{\partial f}{\partial t} + \boldsymbol{v} \cdot \nabla f + \frac{e\boldsymbol{E}}{m_e} \cdot \frac{\partial f}{\partial \boldsymbol{v}} = -J(f), \tag{10}$$

where $\boldsymbol{r}$, $\boldsymbol{v}$, e and m_e denote the position, velocity, charge and mass of the electron, respectively, and $J(f)$ is the collision operator accounting for interactions with the background gas. The scattering cross sections (elastic momentum-transfer, elastic viscosity-transfer, excitations and electron-impact ionization) are included directly in the corresponding collision operator component [16,19].

Assuming weak gradients, the space-time dependence of the phase-space distribution function can be projected onto the number density $n(\boldsymbol{r}, t)$ via the density gradient expansion [21]:

$$
\begin{aligned}
f(\boldsymbol{r}, \boldsymbol{v}, t) = nF(\boldsymbol{v}) - F^L(\boldsymbol{v})\frac{\partial n}{\partial z} \\
&- F^T(\boldsymbol{v})\left[\cos\phi\frac{\partial n}{\partial x} + \sin\phi\frac{\partial n}{\partial y}\right] \\
&+ \sqrt{\frac{1}{3}}F^{2T}(\boldsymbol{v})\left[\frac{\partial^2 n}{\partial x^2} + \frac{\partial^2 n}{\partial y^2} + \frac{\partial^2 n}{\partial y^2}\right] \\
&+ \sqrt{\frac{2}{3}}F^{2L}(\boldsymbol{v})\left[\frac{1}{2}\left(\frac{\partial^2 n}{\partial x^2} + \frac{\partial^2 n}{\partial y^2}\right) - \frac{\partial^2 n}{\partial y^2}\right] \\
&+ \ldots, \qquad (11)
\end{aligned}
$$

where ϕ is the azimuthal angle, and the superscripts L and T define quantities that are parallel and transverse to the electric field, respectively.

The velocity dependence is expanded further in terms of (associated) Legendre polynomials $P_l^m(\cos\theta)$ [22], i.e.,

$$F(\boldsymbol{v}) = \sum_{l=0}^{\infty} F_l(v) P_l^0(\cos\theta), \qquad (12)$$

$$F^{L,2T,2L}(\boldsymbol{v}) = \sum_{l=0}^{\infty} F_l^{L,2T,2L}(v) P_l^0(\cos\theta), \qquad (13)$$

$$F^T(\boldsymbol{v}) = \sum_{l=0}^{\infty} F_l^T(v) P_l^1(\cos\theta), \qquad (14)$$

where θ denotes the angle relative to the electric field direction. Note that P_l^0 are just the standard Legendre polynomials. Boltzmann's equation can then be represented as a hierarchy of equations for these expansion coefficients [23]. A true multiterm approach is used to solve this hierarchy, capturing anisotropic effects in the velocity distribution due to elastic and inelastic scattering. These effects are especially important in systems with significant inelastic energy loss processes [23–25].

In practice, the expansion is truncated at a finite-order l_{max}, which is increased until convergence of the transport coefficients is achieved. In this study, $l_{max} = 7$ was sufficient to ensure convergence within 0.5% across the full reduced electric field range considered, and a detailed discussion is given in Section 3.3.

From the solution of Equations (12)–(14), which includes the scattering cross sections via the collision operator, we compute transport properties including the flux drift velocity (W), mean energy (ϵ), flux longitudinal (D^L) and flux transverse (D^T) diffusion coefficients [23,26]:

$$\epsilon = 2\pi m_e \int_0^{\infty} v^4 F_0(v) dv, \qquad (15)$$

$$W = \frac{4\pi}{3}\int_0^{\infty} v^3 F_1(v) dv, \qquad (16)$$

$$D^{L,T} = \frac{4\pi}{3}\int_0^{\infty} v^3 F_1^{L,T}(v) dv, \qquad (17)$$

which are related to their bulk coefficient counterparts (W_B, D_B^L and D_B^T) via [23,26]:

$$W_B = W - 4\pi \int_0^\infty v^2 \nu_R(v) F_1(v) dv, \tag{18}$$

$$D_B^L = D^L - \frac{4\pi}{\sqrt{3}} \int_0^\infty v^2 \nu_R(v) \left[F_0^{2T}(v) - \sqrt{2} F_0^{2L}(v) \right] dv, \tag{19}$$

$$D_B^T = D^T - \frac{4\pi}{\sqrt{3}} \int_0^\infty v^2 \nu_R(v) \left[F_0^{2T}(v) + \frac{\sqrt{2}}{2} F_0^{2L}(v) \right] dv, \tag{20}$$

where $\nu_R(v)$ is the total reactive collision frequency. In the gaseous radon considered here, the only non-conservative process is electron-impact ionization, and thus, $\nu_R(v) = -\nu_{ion}(v) = -Nv\sigma_{ion}(v)$. The electron mobility, $\mu = W_B/E$, is often reported directly or as a ratio with the bulk diffusion coefficient as a proxy for the mean energy of the system.

It is critical to distinguish between flux and bulk transport coefficients. Flux coefficients represent the average particle behavior, while bulk coefficients describe the motion and spread of the swarm's center of mass. In systems with significant ionization, these coefficients can differ by orders of magnitude and exhibit entirely different behavior. It is the bulk and not the flux transport coefficients which are generally measured and tabulated in the vast majority of the swarm experiment literature [25,27,28].

Finally, the net reaction rate R_{net} is related to the Townsend ionization coefficient, α by the expression

$$R_{net} \approx \alpha W_B - \alpha^2 D_B^L. \tag{21}$$

For ease of comparison with prior work, we report both the net reaction rate and the Townsend ionization coefficient in Section 3.

3. Results and Discussion

3.1. Cross Sections

The electron–radon scattering cross sections for the elastic momentum-transfer, elastic viscosity-transfer, total sum of excitations and electron-impact ionization processes, calculated using the ROP method described in Section 2.1, are shown in Figure 1, along with the calculations from Khandker et al. [2].

The tabulated values derived using the ROP method are presented in Table 1 for energies spanning 0 to 1000 eV. These include the total elastic, momentum-transfer cross section, viscosity-transfer cross section and excitation and ionization cross sections.

In Section 2.3, a comparison of the fully relativistic ROP and semi-relativistic OPM calculation methodologies was given. The ROP and OPM methods differ primarily in their treatment of exchange, polarization and inelastic processes, with the ROP method offering a more physically consistent and fully relativistic approach.

In general, the cross sections show broadly similar trends between the two methods. A notable distinction lies in the treatment of inelastic processes. Khandker et al. [2] report a total inelastic cross section, encompassing both the ionization and excitation channels, without resolving them individually. This total appears to underestimate the ROP ionization cross section, even though it should in principle account for additional excitation contributions. Furthermore, the OPM inelastic cross section shows unphysical behavior at low energies, including contributions below the inelastic thresholds. This arises due to their method of calculating the inelastic cross section as the difference between the total and elastic cross sections, potentially introducing artifacts.

Table 1. A representative selection of the calculated cross sections for total elastic (Elas.), momentum-transfer (MTCS), viscosity-transfer (VTCS), sum of all discrete excitations (Exc.) and electron-impact ionization (Ion.) for electron scattering from radon. Calculations have been performed as described in Section 2.1 and coincide with the profiles shown in Figure 1.

Energy [eV]	**Elas.** [10^{-20}m]	**MTCS** [10^{-20}]	**VTCS** [10^{-20}]	**Exc.** [10^{-20}]	**Energy** [eV]	**Elas.** [10^{-20}]	**MTCS** [10^{-20}]	**VTCS** [10^{-20}]	**Exc.** [10^{-20}]	**Ion.** [10^{-20}]
0	2.72×10^{3}	2.72×10^{3}	1.81×10^{3}	0	10	4.45×10^{1}	1.53×10^{1}	1.46×10^{1}	8.19×10^{-1}	0
1×10^{-3}	2.42×10^{3}	2.41×10^{3}	1.61×10^{3}	0	11	4.33×10^{1}	1.30×10^{1}	1.34×10^{1}	1.00	2.70×10^{-2}
1×10^{-2}	1.32×10^{3}	1.30×10^{3}	8.81×10^{2}	0	12	4.22×10^{1}	1.12×10^{1}	1.22×10^{1}	1.15	2.26×10^{-1}
0.1	2.12×10^{2}	1.94×10^{2}	1.38×10^{2}	0	13	4.13×10^{1}	9.75	1.11×10^{1}	1.27	4.33×10^{-1}
0.2	9.24×10^{1}	7.74×10^{1}	5.82×10^{1}	0	14	4.06×10^{1}	8.74	1.02×10^{1}	1.39	6.27×10^{-1}
0.3	5.22×10^{1}	4.01×10^{1}	3.13×10^{1}	0	15	3.99×10^{1}	8.08	9.30	1.49	8.14×10^{-1}
0.4	3.30×10^{1}	2.33×10^{1}	1.85×10^{1}	0	16	3.92×10^{1}	7.73	8.53	1.59	1.01
0.5	2.22×10^{1}	1.44×10^{1}	1.15×10^{1}	0	17	3.85×10^{1}	7.63	7.86	1.70	1.22
0.6	1.57×10^{1}	9.44	7.23	0	18	3.76×10^{1}	7.74	7.29	1.80	1.43
0.7	1.15×10^{1}	6.55	4.63	0	19	3.66×10^{1}	8.01	6.82	1.90	1.66
0.8	8.89	4.91	3.03	0	20	3.54×10^{1}	8.36	6.44	1.99	1.89
0.9	7.28	4.07	2.12	0	21	3.40×10^{1}	8.75	6.14	2.06	2.12
1.0	6.39	3.79	1.67	0	22	3.25×10^{1}	9.12	5.91	2.12	2.37
1.2	6.10	4.35	1.75	0	23	3.09×10^{1}	9.43	5.71	2.17	2.62
1.4	7.15	5.93	2.68	0	24	2.92×10^{1}	9.64	5.54	2.22	2.87
1.6	9.77	1.03×10^{1}	4.38	0	25	2.76×10^{1}	9.76	5.38	2.26	3.12
1.8	1.18×10^{1}	1.10×10^{1}	5.99	0	30	2.01×10^{1}	9.12	4.59	2.41	4.27
2.0	1.49×10^{1}	1.43×10^{1}	8.07	0	35	1.52×10^{1}	7.71	3.80	2.47	5.15
2.2	1.84×10^{1}	1.77×10^{1}	1.03×10^{1}	0	40	1.22×10^{1}	6.45	3.18	2.45	5.76
2.4	2.22×10^{1}	2.13×10^{1}	1.25×10^{1}	0	45	1.04×10^{1}	5.50	2.75	2.40	6.18
2.6	2.61×10^{1}	2.48×10^{1}	1.47×10^{1}	0	50	9.29	4.80	2.45	2.33	6.47
2.8	2.99×10^{1}	2.81×10^{1}	1.67×10^{1}	0	55	8.57	4.28	2.27	2.27	6.64
3.0	3.35×10^{1}	3.11×10^{1}	1.85×10^{1}	0	60	8.10	3.92	2.13	2.21	6.74
3.2	3.69×10^{1}	3.37×10^{1}	2.00×10^{1}	0	65	7.84	3.58	2.09	2.15	6.80
3.4	4.00×10^{1}	3.58×10^{1}	2.13×10^{1}	0	70	7.68	3.34	2.06	2.10	6.81
3.6	4.26×10^{1}	3.73×10^{1}	2.22×10^{1}	0	75	7.60	3.14	2.05	2.05	6.80
3.8	4.49×10^{1}	3.84×10^{1}	2.29×10^{1}	0	80	7.58	2.97	2.05	1.99	6.77
4.0	4.67×10^{1}	3.90×10^{1}	2.34×10^{1}	0	85	7.58	2.82	2.05	1.93	6.72
4.2	4.82×10^{1}	3.92×10^{1}	2.36×10^{1}	0	90	7.61	2.70	2.06	1.88	6.66
4.4	4.93×10^{1}	3.91×10^{1}	2.37×10^{1}	0	95	7.63	2.58	2.06	1.82	6.59
4.6	5.01×10^{1}	3.87×10^{1}	2.36×10^{1}	0	100	7.67	2.47	2.06	1.77	6.51
4.8	5.07×10^{1}	3.80×10^{1}	2.34×10^{1}	0	110	7.71	2.27	2.03	1.67	6.34
5.0	5.11×10^{1}	3.72×10^{1}	2.31×10^{1}	0	120	7.73	2.09	1.98	1.58	6.17
5.2	5.13×10^{1}	3.63×10^{1}	2.28×10^{1}	0	130	7.71	1.92	1.91	1.50	6.00
5.4	5.13×10^{1}	3.53×10^{1}	2.24×10^{1}	0	140	7.66	1.77	1.82	1.42	5.83
5.6	5.13×10^{1}	3.42×10^{1}	2.21×10^{1}	0	150	7.58	1.64	1.73	1.35	5.67
5.8	5.12×10^{1}	3.31×10^{1}	2.17×10^{1}	0	160	7.49	1.52	1.64	1.29	5.52
6.0	5.10×10^{1}	3.20×10^{1}	2.13×10^{1}	0	170	7.39	1.42	1.56	1.23	5.38
6.2	5.07×10^{1}	3.09×10^{1}	2.09×10^{1}	0	180	7.28	1.34	1.48	1.17	5.24
6.4	5.05×10^{1}	2.99×10^{1}	2.05×10^{1}	0	190	7.17	1.27	1.41	1.12	5.11
6.6	5.02×10^{1}	2.88×10^{1}	2.01×10^{1}	0	200	7.06	1.21	1.36	1.07	4.98
6.8	4.98×10^{1}	2.78×10^{1}	1.97×10^{1}	0	250	6.56	1.05	1.17	9.46×10^{-1}	4.48
7.0	4.93×10^{1}	2.66×10^{1}	1.93×10^{1}	1.63×10^{-1}	300	6.12	1.00	1.07	8.05×10^{-1}	4.03
7.2	4.89×10^{1}	2.55×10^{1}	1.88×10^{1}	3.03×10^{-1}	350	5.74	9.84×10^{-1}	1.00	6.94×10^{-1}	3.65
7.4	4.84×10^{1}	2.45×10^{1}	1.84×10^{1}	3.62×10^{-1}	400	5.42	9.70×10^{-1}	9.36×10^{-1}	6.05×10^{-1}	3.33
7.6	4.81×10^{1}	2.36×10^{1}	1.81×10^{1}	3.94×10^{-1}	450	5.13	9.53×10^{-1}	8.75×10^{-1}	5.33×10^{-1}	3.06
7.8	4.77×10^{1}	2.27×10^{1}	1.77×10^{1}	4.23×10^{-1}	500	4.88	9.32×10^{-1}	8.17×10^{-1}	4.74×10^{-1}	2.82
8.0	4.74×10^{1}	2.19×10^{1}	1.74×10^{1}	4.39×10^{-1}	550	4.66	9.07×10^{-1}	7.62×10^{-1}	4.54×10^{-1}	2.66
8.2	4.70×10^{1}	2.11×10^{1}	1.71×10^{1}	4.53×10^{-1}	600	4.47	8.81×10^{-1}	7.11×10^{-1}	4.11×10^{-1}	2.48
8.4	4.67×10^{1}	2.04×10^{1}	1.68×10^{1}	4.76×10^{-1}	650	4.30	8.54×10^{-1}	6.64×10^{-1}	3.74×10^{-1}	2.32
8.6	4.64×10^{1}	1.96×10^{1}	1.65×10^{1}	5.09×10^{-1}	700	4.15	8.27×10^{-1}	6.22×10^{-1}	3.42×10^{-1}	2.17
8.8	4.61×10^{1}	1.89×10^{1}	1.62×10^{1}	5.87×10^{-1}	750	4.01	8.00×10^{-1}	5.83×10^{-1}	3.14×10^{-1}	2.04
9.0	4.58×10^{1}	1.82×10^{1}	1.59×10^{1}	6.51×10^{-1}	800	3.89	7.73×10^{-1}	5.48×10^{-1}	2.90×10^{-1}	1.92
9.2	4.55×10^{1}	1.76×10^{1}	1.56×10^{1}	6.90×10^{-1}	850	3.78	7.47×10^{-1}	5.17×10^{-1}	2.68×10^{-1}	1.81
9.4	4.52×10^{1}	1.70×10^{1}	1.54×10^{1}	7.24×10^{-1}	900	3.68	7.22×10^{-1}	4.88×10^{-1}	2.49×10^{-1}	1.71
9.6	4.50×10^{1}	1.64×10^{1}	1.51×10^{1}	7.55×10^{-1}	950	3.59	6.98×10^{-1}	4.62×10^{-1}	2.32×10^{-1}	1.62
9.8	4.47×10^{1}	1.59×10^{1}	1.48×10^{1}	7.86×10^{-1}	1000	3.51	6.74×10^{-1}	4.39×10^{-1}	2.17×10^{-1}	1.54

Despite these limitations, the high-energy shape of the OPM inelastic profile aligns reasonably well with that from the ROP method, suggesting some consistency in asymptotic behavior.

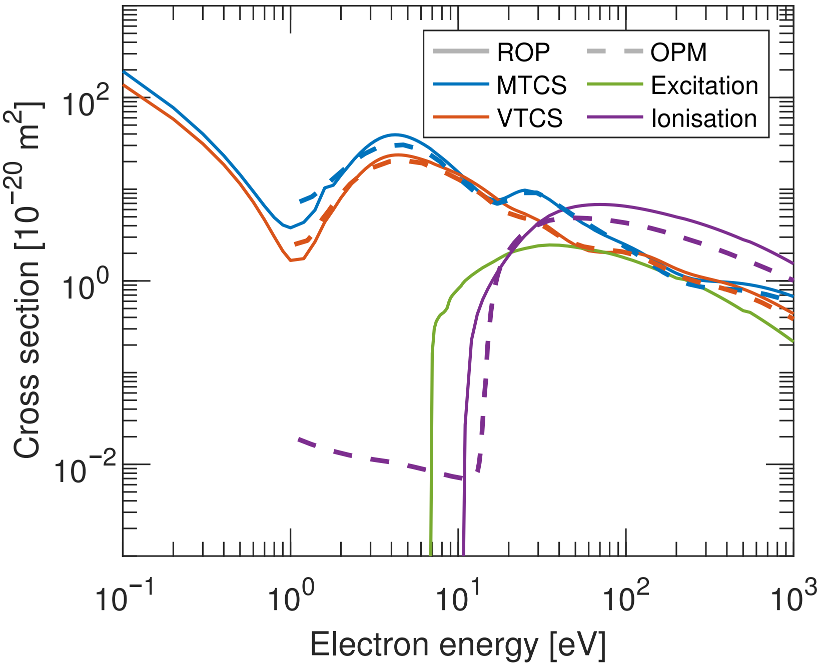

Figure 1. Cross sections for the elastic momentum-transfer (MTCS), elastic viscosity-transfer (VTCS), sum of excitations (excitation) and electron-impact ionization (ionization) processes in radon, those calculated using the ab initio method described in Section 2.1 (ROP, solid lines) and those digitized from Khandker et al. [2] (OPM, dashed lines). The OPM profile labeled "VTCS" has been scaled by a factor of 2/3 to account for the differing definitions of the viscosity-transfer cross section. The OPM profile labeled "Ionisation" is actually the total inelastic cross section, combining excitations and ionization processes, which is calculated from the difference between the total and inelastic cross sections in ref. [2].

3.2. Transport Properties

Figure 2 presents the calculated transport coefficients for an electron swarm in radon gas at 293 K, across a broad range of reduced electric fields (E/N from 0.01 to 1000 Td), using the cross section data from Table 1.

The top left panel shows the bulk and flux drift velocities, derived from the ROP cross section set. Notable divergence between the bulk and flux values emerges above approximately 100 Td, indicative of increasing non-conservative behavior (i.e., ionization).

The top right panel illustrates the transverse and longitudinal characteristic energies ($3D_T/(2\mu)$ and $3D_L/(2\mu)$) alongside the mean energy (ϵ). The transverse characteristic energy is commonly used as a proxy for the mean energy but clearly differs significantly for the case of electron in radon gas for reduced electric fields between approximately 0.1 Td and 100 Td, emphasizing the limitations of using it as a surrogate measure. The longitudinal characteristic energy exhibits a dip between approximately 0.3 Td and 3 Td, corresponding to the mean electron energy increasing beyond the Ramsauer minimum. This behavior is a more pronounced example of the same phenomenon observed for electrons in argon, krypton and xenon [29].

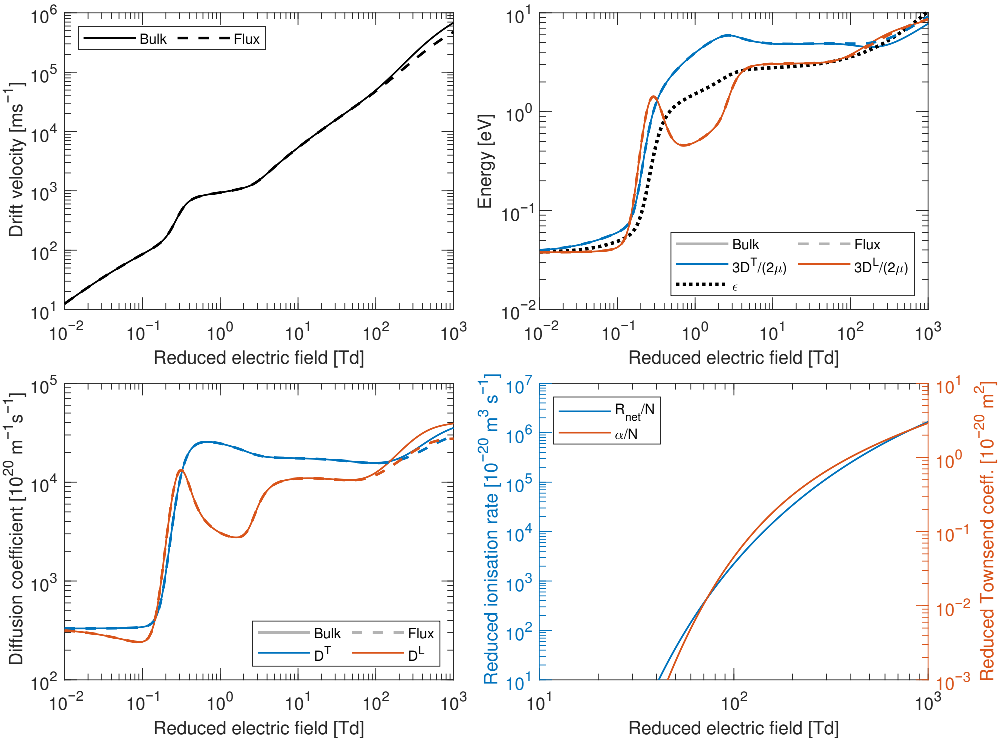

Figure 2. Transport properties calculated using the ab initio cross section set described in Section 2.1 and tabulated in Table 1. The transport properties are defined in Equations (15)–(21). (**top left**) Bulk and flux drift velocities. (**top right**) Transverse and longitudinal characteristic energies (bulk and flux) and the mean energy. (**bottom left**) Transverse and longitudinal diffusion coefficients (bulk and flux). (**bottom right**) Ionization coefficient.

In the bottom left panel, the longitudinal and transverse diffusion coefficients are shown, both in bulk and flux forms. Clear differences are exhibited by the longitudinal and transverse behavior, with divergence between the bulk and flux forms occurring at approximately 100 Td, again reflecting the growing influence of ionization. The longitudinal diffusion coefficient shows a comparable dip to the longitudinal characteristic energy between approximately 0.3 Td and 3 Td, reflecting the same underlying energy-dependent scattering behavior.

Finally, the bottom right panel displays the net reaction rate and, equivalently, the Townsend ionization coefficient, according to Equation (21). The profile clearly indicates the onset and growth of ionization processes as E/N increases.

3.3. Multi-Term

To assess the impact of velocity-space anisotropy, we compared the transport results from the full multi-term solution of Boltzmann's equation to those obtained using the widely adopted "two-term" approximation.

For computational simplicity, the "two-term" approximation is often employed in solving Boltzmann's equation, despite its well-established limitations [24,25,30]. In this work, we use a multi-term Boltzmann solver, as described in Section 2 and in previous works [18–20]: we increment the number of terms until some convergence criterion is met. Here, the criterion is that all reported transport coefficients differ by less than 0.5% with increasing $l_{\max}$, which we found to occur for $l_{\max} = 7$.

Figure 3 quantifies the percentage error introduced by the two-term approximation ($l_{\max} = 1$) relative to the fully converged solution ($l_{\max} = 7$). While the drift velocity remains within 4% of the accurate value, deviations in the diffusion coefficients are far more significant, e.g., up to 15–30% for the transverse and longitudinal components, respectively. This indicates the failure of the two-term approximation for the evaluation of the diffusion coefficients at fields above approximately 10 Td.

These findings reaffirm previous studies (e.g., Brennan and Ness [31]). As such, any effort to adjust the cross sections through inverse swarm techniques must ensure consistency with a multi-term framework, lest the results be biased by an insufficient angular resolution in the velocity distribution function.

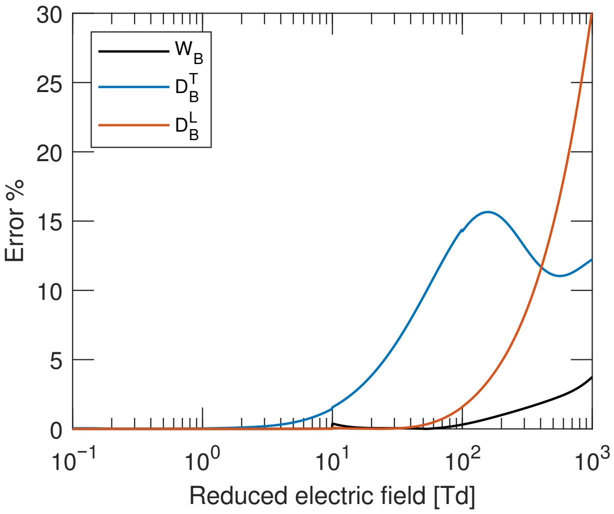

Figure 3. Percentage differences between the two-term ($l_{\text{max}} = 1$) and multi-term ($l_{\text{max}} = 7$) values of the bulk drift velocity, bulk transverse and longitudinal diffusion coefficients. All percentages are relative to the converged multi-term result.

4. Summary

We have presented comprehensive calculations of the electron scattering cross sections and associated transport properties in radon gas, employing a relativistic optical potential (ROP) framework. The ROP method incorporates detailed treatments of exchange, polarization and absorption processes based on the Dirac–Fock atomic structure, enabling accurate and fully relativistic modeling appropriate for this heavy noble gas.

Elastic, momentum-transfer, viscosity-transfer, excitation and ionization cross sections were calculated over a broad energy range (0–1000 eV) and compared against the semi-relativistic OPM results from Khandker et al. [2]. Notable differences were observed, particularly in the low-energy behavior of the inelastic cross sections, where the OPM method exhibited unphysical contributions below the threshold.

Using the ROP cross sections, we solved the Boltzmann equation via a multi-term expansion to obtain transport coefficients across a wide range of reduced electric fields (0.01–1000 Td). We report the drift velocities, diffusion coefficients, mean energy and ionization rates in both bulk and flux forms. The results highlight the importance of multi-term treatments in systems with strong inelastic scattering, as evidenced by significant deviations between two-term and converged solutions for diffusion in moderate and high fields.

The cross section set and transport coefficients provided here represent the first fully relativistic, ab initio dataset for electron–radon scattering and swarm transport. These results offer a reliable foundation for modeling plasmas and radiation transport in radon-rich environments, with implications for detector calibration, radiation safety and atmospheric physics.

Author Contributions: G.J.B.: Conceptualization, Data curation, Formal analysis, Methodology, Project administration, Software, Validation, Visualization, Writing—original draft, Writing—review & editing. D.L.M.: Data curation, Formal analysis, Software, Validation, Visualization, Writing—original draft, Writing—review & editing. J.R.M.: Conceptualization, Data curation, Investigation, Methodology, Project administration, Resources, Validation, Visualization, Writing—original draft, Writing—review & editing. R.P.M.: Conceptualization, Data curation, Investigation, Methodology, Project administration, Resources, Software, Validation, Visualization, Writing—original draft, Writing—review & editing. All authors have read and agreed to the published version of the manuscript.

Funding: J.R.M. and D.L.M. gratefully acknowledge the financial support of the Australian Research Council (ARC) through the Discovery Projects Scheme (J.R.M.: DP200101294, DE160100098; D.L.M.: DP220101480, DP190100696).

Data Availability Statement: A representative selection of data is presented in Table 1. The data will be made available upon reasonable request.

Acknowledgments: The authors also wish to acknowledge the support of the Australian Research Council.

Conflicts of Interest: The authors declare no conflicts of interest.

References

1. Brunger, M.J.; Buckman, S.J.; Allen, L.J.; McCarthy, I.E.; Ratnavelu, K. Elastic electron scattering from helium: Absolute experimental cross sections, theory and derived interaction potentials. *J. Phys. B At. Mol. Opt. Phys.* **1992**, *25*, 1823. [CrossRef]
2. Khandker, M.H.; Haque, A.K.F.; Haque, M.M.; Billah, M.M.; Watabe, H.; Uddin, M.A. Relativistic Study on the Scattering of $e^{\pm}$ from Atoms and Ions of the Rn Isonuclear Series. *Atoms* **2021**, *9*, 59. [CrossRef]
3. Lam, L.T.S.F. Relativistic effects in electron scattering by atoms. III. Elastic scattering by krypton, xenon and radon. *J. Phys. B At. Mol. Phys.* **1982**, *15*, 119. [CrossRef]
4. Neerja; Tripathi, A.N.; Jain, A.K. Spin polarization and cross sections in elastic scattering of electrons from Yb, Rn, and Ra atoms. *Phys. Rev. A* **2000**, *61*, 032713. [CrossRef]
5. Sharma Kapil, K.; Vats, R.P. Elastic positron scattering by radon and radium atoms. *Phys. Scr.* **2012**, *85*, 045304. [CrossRef]
6. Chen, S.; McEachran, R.P.; Stauffer, A.D. Ab initio optical potentials for elastic electron and positron scattering from the heavy noble gases. *J. Phys. B At. Mol. Opt. Phys.* **2008**, *41*, 025201. [CrossRef]
7. McEachran, R.P.; Hamilton, K.R.; Bartschat, K. Low-Energy Elastic Electron Scattering from Helium Atoms. *Atoms* **2021**, *9*, 82. [CrossRef]
8. McEachran, R.P.; Ryman, A.G.; Stauffer, A.D.; Morgan, D.L. Positron scattering from noble gases. *J. Phys. B At. Mol. Phys.* **1977**, *10*, 663. [CrossRef]
9. McEachran, R.P.; Morgan, D.L.; Ryman, A.G.; Stauffer, A.D. Positron scattering from noble gases: Corrected results for helium. *J. Phys. B At. Mol. Phys.* **1978**, *11*, 951. [CrossRef]
10. McEachran, R.P.; Stauffer, A.D. Dynamic distortion effects in electron-atom scattering. *J. Phys. B At. Mol. Opt. Phys.* **1990**, *23*, 4605. [CrossRef]
11. McEachran, R.; Stauffer, A. Relativistic Effects in Low-Energy Electron–Argon Scattering. *Aust. J. Phys.* **1997**, *50*, 511–524.
12. Bartschat, K.; McEachran, R.P.; Stauffer, A.D. Optical potential approach to electron and positron scattering from noble gases. I. Argon. *J. Phys. B At. Mol. Opt. Phys.* **1988**, *21*, 2789. [CrossRef]
13. Bartschat, K.; McEarchran, R.P.; Stauffer, A.D. Optical potential approach to electron and positron scattering from noble gases. II. Neon. *J. Phys. B At. Mol. Opt. Phys.* **1990**, *23*, 2349. [CrossRef]
14. Salvat, F. Optical-model potential for electron and positron elastic scattering by atoms. *Phys. Rev. A* **2003**, *68*, 012708. [CrossRef]
15. Moore, C.E. *Atomic Energy Levels. As Derived From the Analyses of Optical Spectra, Volume 3*; Technical report NSRDS-NBS 35; U.S. Department of Commerce, National Bureau of Standards: Washington, DC, USA, 1958.
16. Robson, R.E.; White, R.D.; Hildebrandt, M. *Fundamentals of Charged Particle Transport in Gases and Condensed Matter*; CRC Press: Boca Raton, FL, USA, 2017.
17. Boyle, G. The Modelling of Non-Equilibrium Light Lepton Transport in Gases and Liquids. Ph.D. Thesis, James Cook University, Townsville, QLD, Australia, 2015.
18. Boyle, G.J.; Tattersall, W.J.; Cocks, D.G.; McEachran, R.P.; White, R.D. A multi-term solution of the space–time Boltzmann equation for electrons in gases and liquids. *Plasma Sources Sci. Technol.* **2017**, *26*, 024007. [CrossRef]

19. Boyle, G.J.; Casey, M.J.E.; Cocks, D.G.; White, R.D.; Carman, R.J. Thermalisation time of electron swarms in xenon for uniform electric fields. *Plasma Sources Sci. Technol.* **2019**, *28*, 035009. [CrossRef]
20. Boyle, G.J.; Stokes, P.W.; Robson, R.E.; White, R.D. Boltzmann's equation at 150: Traditional and modern solution techniques for charged particles in neutral gases. *J. Chem. Phys.* **2023**, *159*, 024306. [CrossRef]
21. Kumar, K.; Skullerud, H.; Robson, R.E. Kinetic theory of charged particle swarms in neutral gases. *Aust. J. Phys.* **1980**, *33*, 343–448. [CrossRef]
22. Abramowitz, M.; Stegun, I. *Handbook of Mathematical Functions*; Dover Publications Inc.: Mineola, NY, USA, 1972.
23. Robson, R.; Ness, K. Velocity distribution function and transport coefficients of electron swarms in gases: Spherical-harmonics decomposition of Boltzmann's equation. *Phys. Rev. A* **1986**, *33*, 2068. [CrossRef]
24. White, R.D.; Robson, R.E.; Schmidt, B.; Morrison, M.A. Is the classical two-term approximation of electron kinetic theory satisfactory for swarms and plasmas? *J. Phys. D Appl. Phys.* **2003**, *36*, 3125. [CrossRef]
25. Petrović, Z.L.; Dujko, S.; Marić, D.; Malović, G.; Nikitović, Z.; Sasić, O.; Jovanović, J.; Stojanović, V.; Radmilović-Radjenović, M. Measurement and interpretation of swarm parameters and their application in plasma modelling. *J. Phys. D Appl. Phys.* **2009**, *42*, 194002. [CrossRef]
26. Yousfi, M.; Segur, P.; Vassiliadis, T. Solution of the Boltzmann equation with ionisation and attachment: Application to SF 6. *J. Phys. D Appl. Phys.* **1985**, *18*, 359–375. [CrossRef]
27. Robson, R. Transport phenomena in the presence of reactions: Definition and measurement of transport coefficients. *Aust. J. Phys.* **1991**, *44*, 685–692. [CrossRef]
28. Casey, M.J.E.; Stokes, P.W.; Cocks, D.G.; Bošnjaković, D.; Simonović, I.; Brunger, M.J.; Dujko, S.; Petrović, Z.L.; Robson, R.E.; White, R.D. Foundations and interpretations of the pulsed-Townsend experiment. *Plasma Sources Sci. Technol.* **2021**, *30*, 035017. [CrossRef]
29. Pack, J.L.; Voshall, R.E.; Phelps, A.V.; Kline, L.E. Longitudinal electron diffusion coefficients in gases: Noble gases. *J. Appl. Phys.* **1992**, *71*, 5363–5371. [CrossRef]
30. Robson, R.E.; Kumar, K. On the validity of the two-term approximation of the electron distribution function. *Aust. J. Phys.* **1971**, *24*, 835–840. [CrossRef]
31. Brennan, M.; Ness, K. Momentum Transfer Cross Section for e–Kr Scattering. *Aust. J. Phys.* **1993**, *46*, 249–260. [CrossRef]